Experimental study on flow phenomena induced by trailing edge shapes for a transonic high pressure turbine cascade

Ines Gohl[1], Martin Bitter[1], Hiroki Sato[2] and Dragan Kožulović[1]

[1]Institute of Jet Propulsion
University of the Bundeswehr Munich
Werner-Heisenberg-Weg 39, 85579 Neubiberg, Germany
ines.gohl@unibw.de, +49 (0)89 6004 3536

[2]IHI Corporation, Japan

ABSTRACT

The present study focuses on the influence of the trailing edge shape and on the development of coherent structures in the transonic flow of a turbine blade passage. Experiments were performed in the High-speed Cascade Wind Tunnel of the University of the Bundeswehr Munich on a high pressure turbine linear cascade. Engine-relevant flow conditions are examined at a constant exit Reynoldys number of Re_{2th} = 1,200,000 and a range of exit Mach numbers from Ma_{2th}= 0.80 to 1.10. The aerodynamic characteristics of the highly unsteady flow is qualitatively investigated using a five hole wedge probe and Particle Image Velocimetry (PIV). By means of a Proper Orthogonal Decomposition (POD) analysis, dominant flow structures are extracted. The near wake flow and shear layer dynamics as well as the evaluation of the wake downstream of the two trailing edge designs are examined. The results show performance benefits due to the mitigation of coherent structures for exit Mach numbers below Ma_{2th}= 1.00 for the profiled trailing edge geometry. For higher exit Mach numbers the round trailing edge has a performance advantage as the strength of the main shock increases and seems to play a dominate role on the integral losses.

NOMENCLATURE
Symbols

c	chord length
c_p	pressure coefficient
div	divergence $\nabla = \frac{\partial u}{\partial x} + \frac{\partial v}{\partial y}$
h	blade height
l_f	vortex formation length
Ma	Mach number
p	pressure
Re	Reynolds number
T	temperature
TI	turbulence intensity
u, v	velocity components
V	velocity magnitude
x, y	cartesian coordinates

Greek letters

β	flow angle
λ	wave length
ω	vorticity $\omega = \frac{\partial v}{\partial x} - \frac{\partial u}{\partial y}$
π	blowing ratio
ζ	(mixed-out) loss coefficient $\zeta = \frac{p_{t1}-p_{t2}}{p_{t1}-p_{Ves}}$

Abbreviations

DEHS	Di-Ethyl-Hexyl-Sebacate
FoV	Field of View
HGK	High-speed Cascade Wind Tunnel
MWP	Miniaturized Wedge Probe
Nd:YAG	Neodymium-doped Yttrium Aluminum Garnet
RTE	Round Trailing Edge
PIV	Particle Image Velocimetry
POD	Proper Orthogonal Decomposition
PPT	Profile Pressure Tabs
PS	Pressure Side
PTE	Profiled Trailing Edge
SEG	Wind Tunnel for Probe Calibration
SS	Suction Side
sCMOS	scientific Complementary Metal-Oxide-Semiconductor
SWBLI	Shock Wave Boundary Layer Interaction
TKE	Turbulent Kinetic Energy

Subscripts

1	inlet plane
2	exit plane
ax	axial
c	cooling air
int	integral
ref	reference
t	total state
th	theoretical (isentropic condition)
Ves	vessel
z	spanwise direction

INTRODUCTION

Resembling the transition from sub- to supersonic flow, one characteristic of transonic flow is its unsteadiness. When increasing the exit Mach number from a subsonic to a transonic, the known isobaric pressure region vanishes and a highly non-uniform pressure distribution is formed at the trailing edge, see Sieverding et al. [1, 2]. The non-uniformity of the trailing edge pressure distribution is caused by transient vortex shedding occurring directly in the base region. Additionally, the classical von Kármán vortex street present in subsonic flow was discovered to be only one of the transient shedding mechanisms when the exit Mach number is raised to transonic. For example, Bölcs and Sari [3] found that in

the subsonic Mach number range, no shocks are observed and the familiar alternating von Kármán vortex street is typically present. In the transonic regime, however, an open unstable base flow region is formed. It is characterized by oscillating normal shocks attached to and transported downstream by the alternating shed vortices.

One factor with crucial impact on the loss production in the wake flow regime is the trailing edge geometry. Consequently, trailing edge shapes have been subject to many investigations, e.g. Prust and Bartlett [4] and Laskowski et al. [5]. El-Gendi et al. [6] demonstrated by using numerical methods that the trailing edge shape has a considerable effect on the base pressure. They revealed that the base pressure for elliptical trailing edges is higher compared to a circular one resulting in lower loss levels. Melzer and Pullan [7] examined different trailing edge geometries for subsonic and transonic exit Mach numbers. They discovered transonic vortex shedding occurring behind blunt trailing edges being the dominant loss generating phenomenon. Each time a vortex is shed at the trailing edge, an acoustic pressure wave is formed which propagates upstream. If the expansion around the trailing edge into the base region is supersonic the pressure wave will form a shock wave. Also, it was found that elliptical trailing edges suppress transonic vortex shedding and therefore are featuring performance advantages over circular and rectangular trailing edge geometries. The effect of the trailing edge shape for a cooled transonic cascade was studied experimentally and numerically by Granovskiy et al. [8]. They found that the losses of a flat trailing edge are twice as high as for a round trailing edge shape. Coherent structures in a transonic high pressure turbine were also contemplated by Lin et al. [9]. By means of high-speed Schlieren imaging, Gohl et al. [10] have studied a cooled conventional and a profiled trailing edge design. They have shown that the profiled trailing edge mitigates the emission of acoustic waves. This significantly changed the passage shock system. The acoustic wave generated at the pressure side of the trailing edge propagate trough the passage to the adjacent blade suction side and there can lead to the emergence of an oblique shock.

The aim of this paper is to gain further qualitative insight and to improve the understanding of the physical mechanism of the unsteady aerodynamic phenomena of the two trailing edge shapes. Special attention is paid on the wake evolution as well as the effects of the acoustic waves on the on the passage flow shock system.

EXPERIMENTAL METHODOLOGY

All measurements presented in this paper were conducted in the High-speed Cascade Wind Tunnel (HGK) at the Institute of Jet Propulsion of the University of the Bundeswehr Munich. The HGK test facility is a continuously operating wind tunnel with an open test section. A cylindrical pressure chamber contains the entire wind tunnel. Thus an independent variation of Mach and Reynolds number can be realized. A detailed description of the test facility can be found in Niehuis and Bitter [11].

Linear cascade

In Fig.1 the wind tunnel test section with the investigated high pressure turbine cascade built-in is sketched. The cascade consists of 5 blades with an axial chord length of about c_{ax} = 110 mm and a blade height h = 300 mm. Two-dimensional flow at midspan of the blade can be assumed with a resulting aspect ratio of h/c = 2.14. The three middle blades are interchangeable and allow for the ejection of cooling air. The two outer blades (numbered 1 and 5) are solid and no cooling air can be ejected. Variable guide vanes whose profiles correspond to the investigated profiles camber line are installed on the upper and lower test section endwall in a distance of approximately half pitch from the preceding blade. At both cascade sidewalls Schlieren windows are installed allowing for optical access. They are located such that the suction side passage flow of the center blade is visible while at the same time the trailing
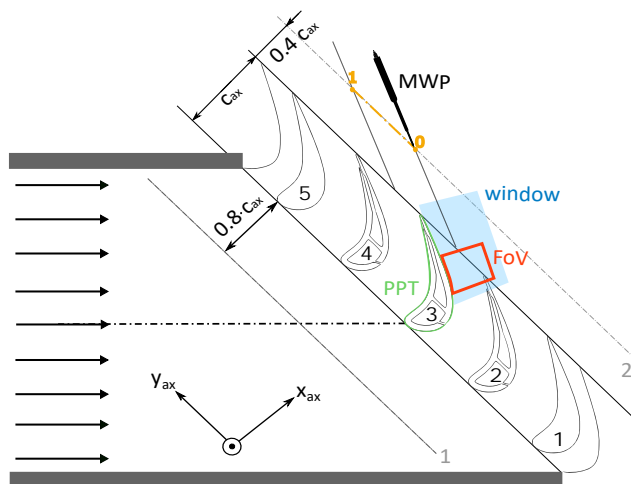

Fig.1 Test section with investigated cascade built in (not to scale).

edge of the adjacent blade can be observed. Each of the middle blades is equipped with two plena which are both connected to a row of cooling hole. One cooling hole row is located at the profile suction side upstream of the throat and consists of 15 laid back fan-shaped cooling holes. The second row is formed by 7 cooling slots positioned pressure sided at the trailing edge. The cooling slots geometry corresponds to straight cut-back slots. Atmospheric air was used as air supply for the cooling air. Cooling air is fed to the plena from both sides of the blade to ensure highly uniform blowing conditions over the blade height. The two investigated profiles are entirely identical except for the trailing edge geometry. In Fig.2, a comparison of the two trailing edge shapes is depicted. The conventional profile is designed with a round trailing edge (RTE) and the modified profile with a so-called profiled trailing edge (PTE). The PTE shape differs from the RTE geometry solely on the profile suction side such that it is thinner. On the pressure side the two trailing edge shapes are congruent. Details about the two trailing edge geometries can be found in patent [12].

The cascade center blade (blade number 3 in Figure 1) is equipped with a total of 42 static Profile Pressure Taps (PPT). The taps are distributed such that 27 taps are positioned on the suction side and 14 taps on the pressure side. One tap is located at the trailing edge measuring the base pressure. In order to determine the profile pressure distribution without disturbing the wake measurements, the taps are placed slightly off mid-span. Furthermore, all cooling plena are equipped with total pressure taps. The plena of the center blade are additionally equipped each with one temperature sensors such that the cooling air blowing conditions can be monitored.
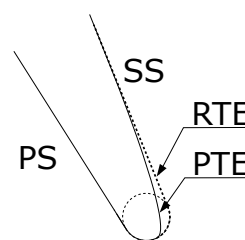

Fig.2 Design of the two investigated trailing edge shapes (not to scale): dashed line - round trailing edge (RTE) and straight line - profiled trailing edge (PTE).

The presented investigation was carried out at a constant theoretical exit Reynolds number of $Re_{2th} = 1,200,000$ at seven exit Mach numbers covering the transonic flow range from $Ma_{2th} = 0.80$ to 1.10. Cooling air was ejected for all operating points by adjusting the total pressure in the plena p_{tc} with respect to the local static pressure p_x. For the trailing edge blowing ratio π as reference pressure p_x the chamber pressure p_{Ves} which corresponds to the exit static pressure p_2 to determine the blowing was used. The measured operating points are presented in Table 1. The inlet temperature of the main flow T_{t1} and cooling air temperature T_{tc} were both set to 303.15 K realizing iso-thermal conditions. The inlet turbulence intensity is estimated to be around $TI_1 = 6\%$.

Table 1 Investigated operating points

Ma_{2th} [-]	Re_{2th} [-]	π_{SS} [-]	π_{TE} [-]
0.80	1,200,000	2.01	1.44
0.90	1,200,000	2.10	1.57
0.94	1,200,000	2.10	1.64
1.00	1,200,000	2.10	1.64
1.05	1,200,000	2.10	1.64
1.10	1,200,000	2.10	1.64

Pressure measurements

The local pressure from the PPTs is used to calculate the pressure coefficient c_p:

$$c_p = \frac{p(x) - p_{Ves}}{p_{t1} - p_{Ves}} \qquad (1)$$

Wake traverse measurements were conducted at 40 % axial chord length downstream of the linear cascade. The covered traverse corresponds to one pitch behind the measurement blade (blade 3) centered around the trailing edge and is located at midspan. The resulting traverse plane is highlighted orange in Fig.1. The utilized five hole probe is a Miniaturized Wedge Probe (MWP) which was optimized for transonic wake flow measurements. The MWP calibration was conducted at the Wind Tunnel for Probe Calibration (SEG) from the Institute of Propulsion Technology at the German Aerospace Center in Göttingen and convers a Mach number range from 0.5 to 1.6 and pitch angles of ±16°. More details about the MWP can be found in Börner and Niehuis [13]. The traverse resolution corresponded to 51 measurement points equidistantly distributed. From the MWP measurements the integral total pressure loss coefficient ζ_{int} is calculated as the mixed-out value according to the method of Amecke [14] under consideration of mass and momentum conservation.

The only absolute pressure measured is the ambient pressure which is recorded by Mensor CPG2500. This precision pressure transducers has an operating range of 552 - 1,172 hPa and the measurement uncertainty amounts to 0.01 % of full-scale range. All other pressures are measured using differential pressure transducers. For the PPTs a Netscanner 98RK rack mount pressure scanner was used with a ±345 hPa pressure module which has a maximum uncertainty of 0.05 % of full-scale range. The wake traverses were recorded using the 9116 pressure scanner by PSI Pressure System with an operating range of ±345 hPa and a maximum uncertainty of 0.05 % of full-scale range. All pressure systems were sampled with a frequency of 10 Hz and averaged over a period of 10 s.

PIV measurements

A planar PIV (2C2D-PIV) system was applied to investigate the flow according to the Field of View (FoV) in Fig.1. For illumination the Nd:YAG double pulse laser INNOLAS Spitlight 1000 with approximately 500 mJ per pulse was used. It is placed outside the pressure chamber and the laser beam is guided through a glass window into the test section. Besides the laser, two PIVTEC seeding generators were installed outside the pressure chamber. DEHS seeding particles of approximately 1 μm were produced into two seeding volumes. With the evacuation of the pressure chamber a pressure gradient exists and thus the seeding is sucked into the flow when the desired operating point is reached. The use of two seeders allowed to seed both the main and cooling air flow. For PIV recording, the LaVision Imager sCMOS camera with a resolution of 2560 X 2160 px and a frame rate of 15 fps was used. The camera setup was installed such that most of the suction side passage flow of the center blade as well as the adjacent trailing edge and its wake. The measurement recording time for each operation point corresponded to almost 8 min. The PIV images were evaluated using the LaVision Davis 10.2 software. After preprocessing a multi-pass PIV algorithm with a 64 x 64 px interrogation windows size and 75 % overlap in combination with subpixel window shift were applied. The resulting spatial resolution is one velocity vector per 0.4 mm. The PIV velocity fields presented here are ensemble-averaged over about 6800 frames.

RESULTS AND DISCUSSION

Loss measurements

The mixed-out integral loss coefficient calculated according to Amecke [14] for the two trailing edge designs is depicted in Fig.3. The illustrated loss is shown for a transonic Mach number range and normalized to the $Ma_{2th} = 0.94$ loss coefficient measured for RTE. It can be seen that the PTE exhibits performance benefits from exit Mach numbers $Ma_{2th} = 0.80$ to 1.00. For exit Mach numbers higher than $Ma_{2th} = 1.00$ RTE performs slightly better than PTE. Additionally, the normalized integral exit flow angles are shown on the lower plot of Fig.3. It is obvious that the trailing edge shape has no severe influence on the integral exit flow angle. The following investigation is focused on elucidating the mechanisms responsible for the loss behavior. Therefore, the passage flows of a subsonic and supersonic exit Mach number are examined more closely. Exemplary, $Ma_{2th} = 0.94$ where shocks are apparent for the first time and PTE exhibits performance benefits compared to RTE, and $Ma_{2th} = 1.10$ where RTE performs better than PTE are chosen.
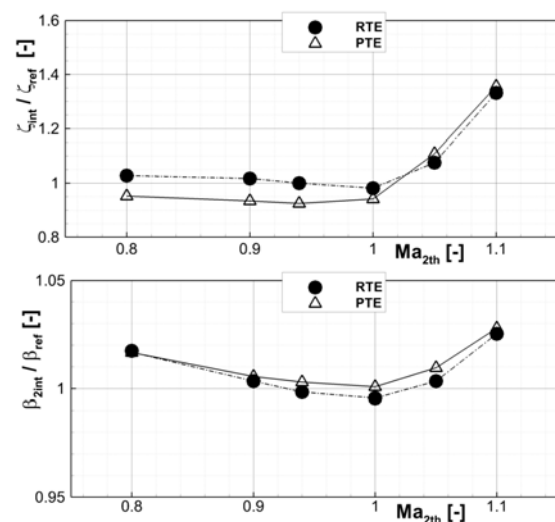

Fig.3 Normalized integral mixed-out pressure loss coefficient (top) and normalized integral exit flow angels (bottom) for RTE and PTE.
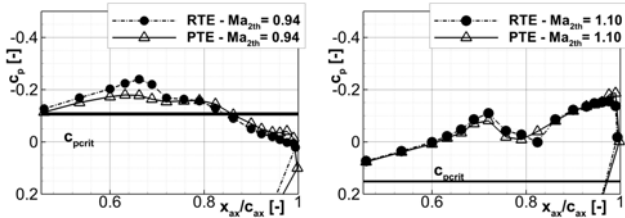
Fig.4 Rear part of the profile pressure distribution at exit Mach numbers Ma_{2th} = 0.94 and 1.10 (left to right). Empty symbols correspond to PTE and full symbols to RTE.

Profile pressure distribution

The rear part of the suction side profile pressure distributions for the two exit Mach numbers Ma_{2th} = 0.94 and 1.10 are shown in the left and right image of Fig.4, respectively. At Ma_{2th} = 0.94 the pressure distribution of RTE is characterized by a suction peak at approximately 63 % axial chord which correlates with the maximum velocity. The peak is followed by a sudden and short drop which continues until about 66 % axial chord. The following deceleration is less steep and the flow is continuously decelerated towards the trailing edge. At around 82 % axial chord the critical pressure coefficient is crossed. Two differences between the two trailing edge shapes are apparent. The first distinction occurs at the suction peak where the flow is accelerated less for PTE than for RTE. Thereafter the deceleration is less steep for PTE than for RTE such that the two distributions overlap until 100 % axial chord. Here the base pressure tap is located indicating that PTE has a higher base pressure than RTE.

At Ma_{2th} = 1.10 the flow on the rear part of the suction side stays entirely supersonic which means that the terminating main shock is already located aft the profile on the base region for both trailing edge shapes. The pressure distributions for the two trailing edge shapes are very similar and possess two velocity peaks. The first peak is located at about 70 % axial chord length and the second peak just before the base pressure tap. At around relative 70 to 80 % chord length a declaration takes place. When comparing the distributions for the trailing edge designs one minor difference in the region of the declaration at about 81 % relative chord is noticeable where the flow is decelerated slightly more for RTE.

Passage flow characterization

In Fig.5 the normalized velocity contours at exit Mach number Ma_{2th} = 0.94 are presented for RTE, PTE and the Δ RTE-PTE (from left to right), as measured by PIV. The most apparent feature for RTE (left) is the wake velocity deficit of the adjacent blade which expectantly is decaying with growing distance to the trailing edge. A low velocity region wrapping around the adjacent blade's trailing edge is also detectable. Additionally, on the measurement blade suction side around 65-77 % relative chord length the peak velocity is reached. The shape of the velocity peak contour (marked A) corresponds to a triangle that is gradually stretching into the passage until approximately 75 % relative axial chord and than relatively abruptly terminates. Around this peak triangle the contour lines curvature is present which bend toward the adjacent blade trailing edge. In the middle of Fig.5 the velocity contours for PTE are illustrated. As for RTE, the wake deficit of the adjacent blade and the suction side velocity peak can be identified. The velocity peak triangle (marked A) is stretched over a longer profile length but is reduced in its extension into the passage flow in comparison to RTE. The curvature of the contour lines toward the adjacent blade trailing edge is also present but less pronounced than for RTE. The normalized velocity difference between the RTE and PTE velocity field is shown on the right hand side of
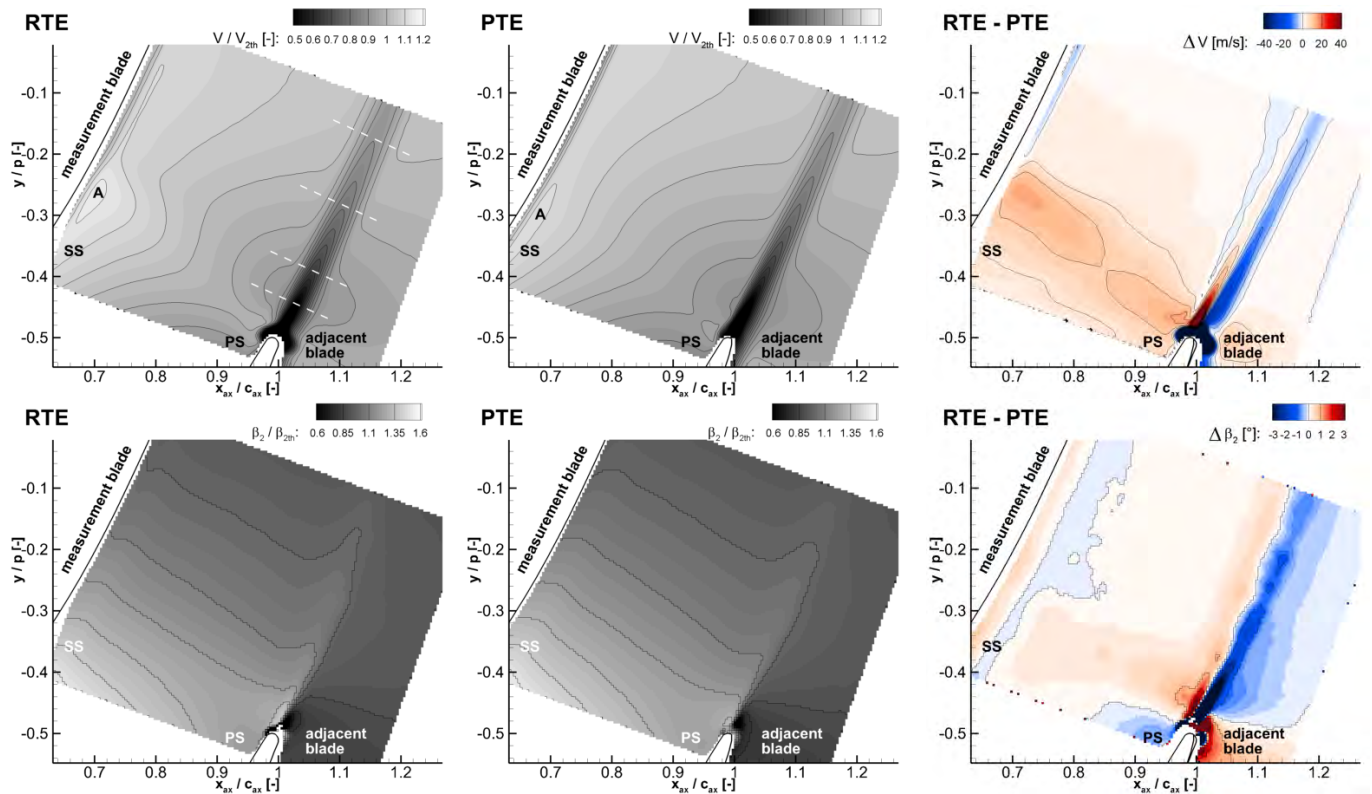

Fig.5 Normalized velocity contours V/V_{2th} (upper row) and flow angle contours β/β_{2th} (lower row) of RTE, PTE and the Δ RTE - PTE (from left to right) at Ma_{2th} = 0.94.
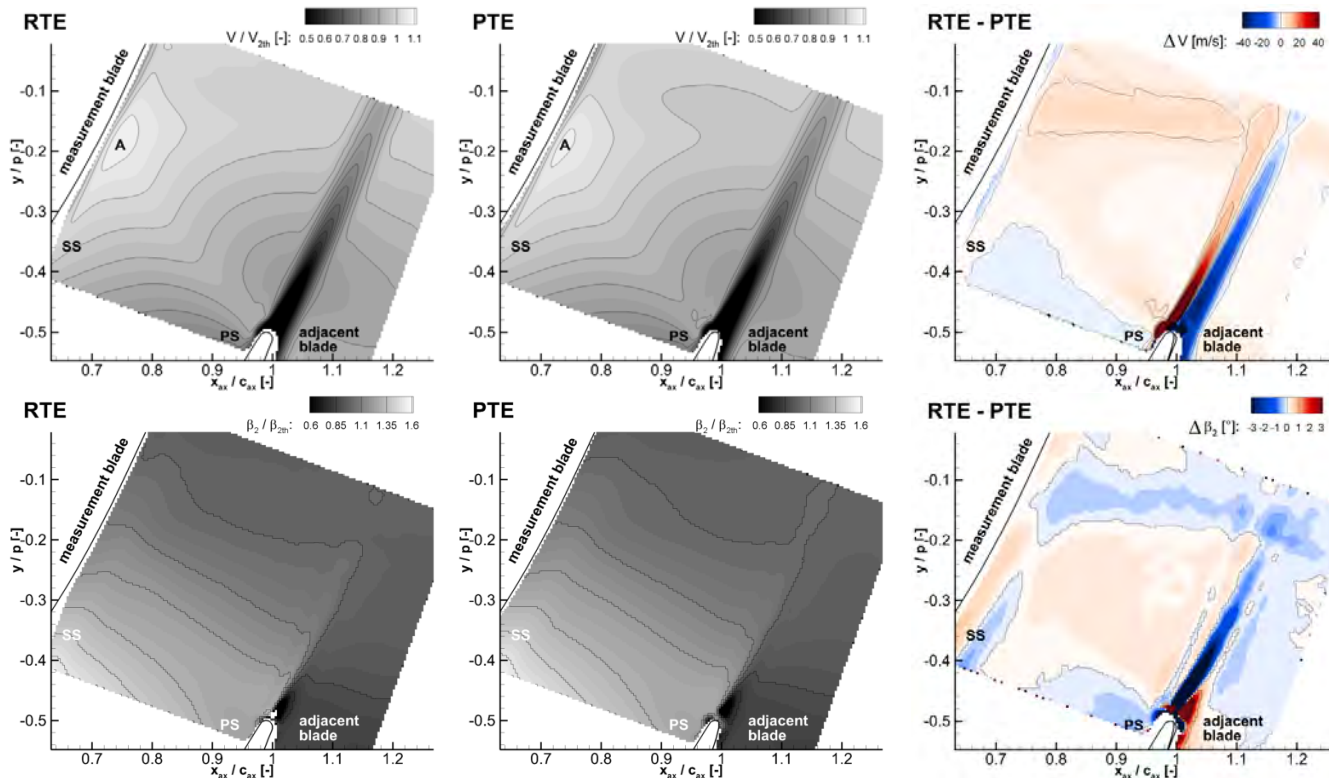
Fig.6 Normalized velocity contours V/V_{2th} (upper row) and flow angle contours β/β_{2th} (lower row) of RTE, PTE and the Δ RTE - PTE (from left to right) at Ma_{2th} = 1.10.

Fig.5. Red contours mean that the RTE exhibits higher velocities and vice versa blue corresponds to higher velocities for PTE. The most dominate difference is visible in the wake of the adjacent blade. Especially around the adjacent blade trailing edge and on the wake suction side PTE posses velocity profits. This difference is attributed to less shear layer movement and a slightly smaller wake width for PTE due to the smaller PTE diameter on the suction side. Whereas on the wake pressure side the RTE flow displays higher velocities. Another distinction is apparent in the throat region (c.f. white ellipse lower row, left side), where over the entire passage height higher velocities are present for RTE. This is in accordance with the blade pressure distribution, c.f. Fig.4. The highest velocities over the passage are reached for RTE at the position of the shear layer movement at the adjacent trailing edge while for PTE the throat starts marginally further upstream and is spanned over a slightly taller region. Therefore, the shear layer movement at the adjacent trailing edge seems to contract the passage flow area and thus determines the position of the throat and leads to slightly higher velocities for RTE. When looking at the normalized flow angle contours in the lower row of Fig.5 of RTE (left) and PTE (middle), it can be seen that the flow is continuously turned towards the trailing edge for both trailing edge designs. The contours correspond to straight lines extending almost over the entire passage height and bend only close to measurement blade boundary layer as well as the adjacent blade wake. As in the velocity fields, no discontinuities are apparent. In the comparison of the two trailing edge flow angle fields (right) red color means higher flow angles for RTE and thus corresponds to less turning and vice verse. It is revealed that besides the differences in the wake higher flow angles i.e. less turning is present for RTE downstream of the adjacent blade trailing edge.

Fig.6 displays the normalized velocity contours at exit Mach numbers Ma_{2th} = 1.10 for RTE, PTE and the Δ RTE-PTE (from left to right). Starting with the RTE velocity contours, the velocity deficit embracing the adjacent trailing edge is not visible anymore at Ma_{2th} = 1.10. The confluence point of the wake where the pressure and suction side boundary layer meet and which terminates the base region cannot clearly be identified. However on the wake pressure side there seems to be a small kink shortly downstream of the adjacent blade trailing edge. The suction peak has moved further upstream to about 75 % to 81 % axial chord and has taken a trapezoid like shape (marked A). For PTE (middle) the shape and location of the suction peak seems almost identical to RTE. In total, the two velocity fields seem very similar. This is confirmed by the comparison of the two flow contours (right) which brings forward that the most dominant distinction takes place in the wake and only small differences are detectable in the passage.

In the lower row of Fig.6, the normalized flow angle contours at Ma_{2th} = 1.10 are depicted for RTE, PTE and the Δ RTE - PTE (from left to right). For both trailing edge shapes the flow is continuously turned towards the trailing edge over the passage height. The contour lines are bend towards the measurement blade suction side and the wake of the adjacent blade. The comparison shows that the main difference is located in the adjacent blade wake suction side. Additionally, the RTE shocks are visible as the flow is turned discontinuously leading to locally higher turning for PTE (blue color).

The analysis of the PIV mean flow distributions, so far, highlights that the two trailing edge shapes investigated mainly influence two regions of the flow: At both investigated exit Mach numbers the main impact of the trailing edge shape was detected to be the wake region. The second affected region was identified to be the base region and throat. Latter is especially true at exit Mach number Ma_{2th} = 0.94. As the wake displays the most prominent difference a closer look is taken at the downstream evolution of the wake.
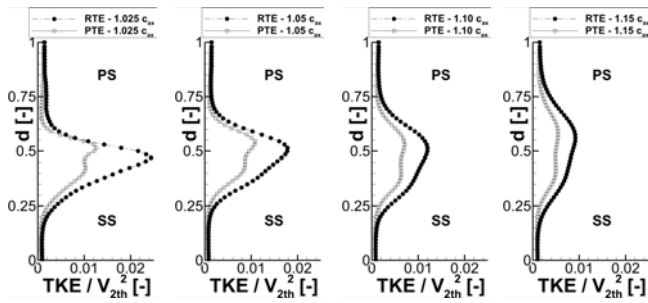
Fig.7 Normalized TKE evolution in the wake of the two trailing edge designs at $Ma_{2th} = 0.94$.

Fig.8 Normalized TKE evolution in the wake of the two trailing edge designs at $Ma_{2th} = 1.10$.

Wake evolution

Besides profile and shock losses, the losses generated in the wake are one of the main contributors to the pressure loss coefficient due to high velocity fluctuations, turbulence and dissipation. The turbulent kinetic energy (TKE) as a measure for turbulent activity is used to describe the downstream evolution of the wake. The TKE development in the wake is visualized in Fig.7 at $Ma_{2th} = 0.94$ and in Fig.8 at $Ma_{2th} = 1.10$. The profiles were extracted at the dashed white lines illustrated in Fig.6 and are located along the wake axis at a distance of about [2.5, 5, 10 and 15] % axial chord length downstream of the trailing edge. At $Ma_{2th} = 0.94$ at all regarded wake section RTE has a higher TKE than PTE. For both trailing edge shapes the TKE decreases and the profile becomes flatter with growing distance to the trailing edge. This is expected as the viscous dissipation and diffusion between the shear layers is more advanced. Looking at the TKE profiles the dominance of the pressure side vortex can also be seen as the TKE peak is shifted towards the pressure side. If the gradients are taken as measure for the wake width then PTE has a slightly smaller wake. This seems to be more pronounced on the suction side. A fact that is important also explaining the lower integral pressure loss for PTE. At $Ma_{2th} = 1.10$ the TKE for the first two sections is about the same for the two trailing edge shapes. In the last two section slightly less TKE can be observed for PTE than for RTE. The dominance of the pressure side vortices is reflected here, too. Additionally, the suctions side vortex seems to contain almost as much TKE as the pressure side vortex in the first section for PTE. Also, at this exit Mach number the wake width for PTE is slightly smaller on the suction side of the wake.

The TKE evolution at exit Mach number $Ma_{2th} = 0.94$ illustrates that clearly less TKE is present for PTE than for RTE which correlates with the loss behavior. With increasing exit Mach number the TKE in the wake is almost the same for the two trailing edge shapes with little advantage for the PTE. Therefore, the pressure loss measured cannot be explained solely by the wakes turbulence. In order to get an understanding of the wake composition as well as the structural sizes involved and to extract the driving mechanisms explaining the loss behavior, a proper orthogonal decomposition is conducted in the following.

Proper Orthogonal Decomposition of the passage flow

About 6,800 PIV fields were used for a POD analysis following the procedure of the method of snapshots. For a detailed description of the POD algorithm the reader is referenced to e.g. Sirovich [15]. The advantage of a POD analysis is that a large amount of energy is contained by a few eigenmodes and thus a complex flow field can be approximated using only a low number of modes. Besides decomposing the flow field into single modes, POD allows for the extraction of characteris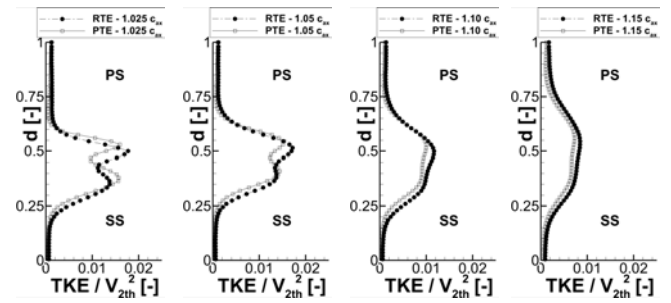tic flow features which are otherwise potentially difficult to identify. The mean subtracted velocity fields were used to compute the POD modes which therefore capture the kinetic energy of the flow fields. As this study is focused on flow regions affected by the trailing edge shape, single modes capturing the same mechanism are selected and compared for the two trailing edge designs. The selected modes dominance and therefore energy contents do not necessarily match.

The raw PIV images display the chaotic turbulent character of the wakes and periodical, defined vortical structures were difficult to identify (not shown here). As the wake is composed of large organized turbulent motion of coherent vorticity concentration, the wake topology is best described using vorticity and divergence. The spatial POD modes which capture the wake structure at exit Mach number $Ma_{2th} = 0.94$ are shown in Fig.9 for RTE, PTE and Δ RTE-PTE (from left to right) by means of vorticity ω_z and divergence. Clearly the POD modes reveal that vortex streets are present and consist of vortex pairs which are ordered in alternating fashion as is known from the von Kármán street for both trailing edge shapes. For RTE the vortex formation starts in a distance (l_f) of approximately one RTE trailing edge diameter as marked by the arrow. For PTE the base region extends further downstream and the vortex formation is delayed in comparison to RTE. The vortex street starts at a distance of about 2 times the PTE trailing edge diameter. The delay of the vortex formation is expected for PTE. The PTE geometry corresponds to a somewhat elliptical shape. The flow around elliptical trailing edge stays longer attached and after separating from the profile the shear layers do not immediately roll up into a vortex but remain stable, as demonstrated by Melzer and Pullan [7]. Additionally, a vortex on the suction side of the adjacent blade is present for the PTE which is not visible for RTE. Regarding the vortex size it is obvious that the PTE vortics are smaller and their lateral displacement is shrunk compared to RTE. As the PTE has a slightly smaller trailing edge diameter than RTE this can be expected. The comparison of the wake structure on the right of Fig.9 by means of the vorticity magnitude confirms this impression. Furthermore, higher vorticity and consequently stronger vortices on the wake pressure side compared to the suction side vortices can also be seen. The dominance of the pressure side vortex is the case for both trailing edge designs and fits to observations made in literature by e.g. Han and Cox [16], or Lawaczeck and Heinemann [17]. Taylor's frozen turbulence hypothesis suggests that all turbulent eddies are advected by the mean streamwise velocity. Thus, the temporal response at a fixed point in space can be regarded as the result of a spatial pattern convecting uniformly past the point with mean streamwise velocity. In the following, Taylor's hypothesis is applied to approximate the vortex shedding frequency by relating the vortices wavelength λ and its convection velocity. The wavelength λ can be extracted from the POD modes as is exemplary shown for RTE in Fig.9. As convection velocity the local mean velocity is derived. Thus, the resulting vortex shedding frequency for RTE is estimated to about 25 kHz and for
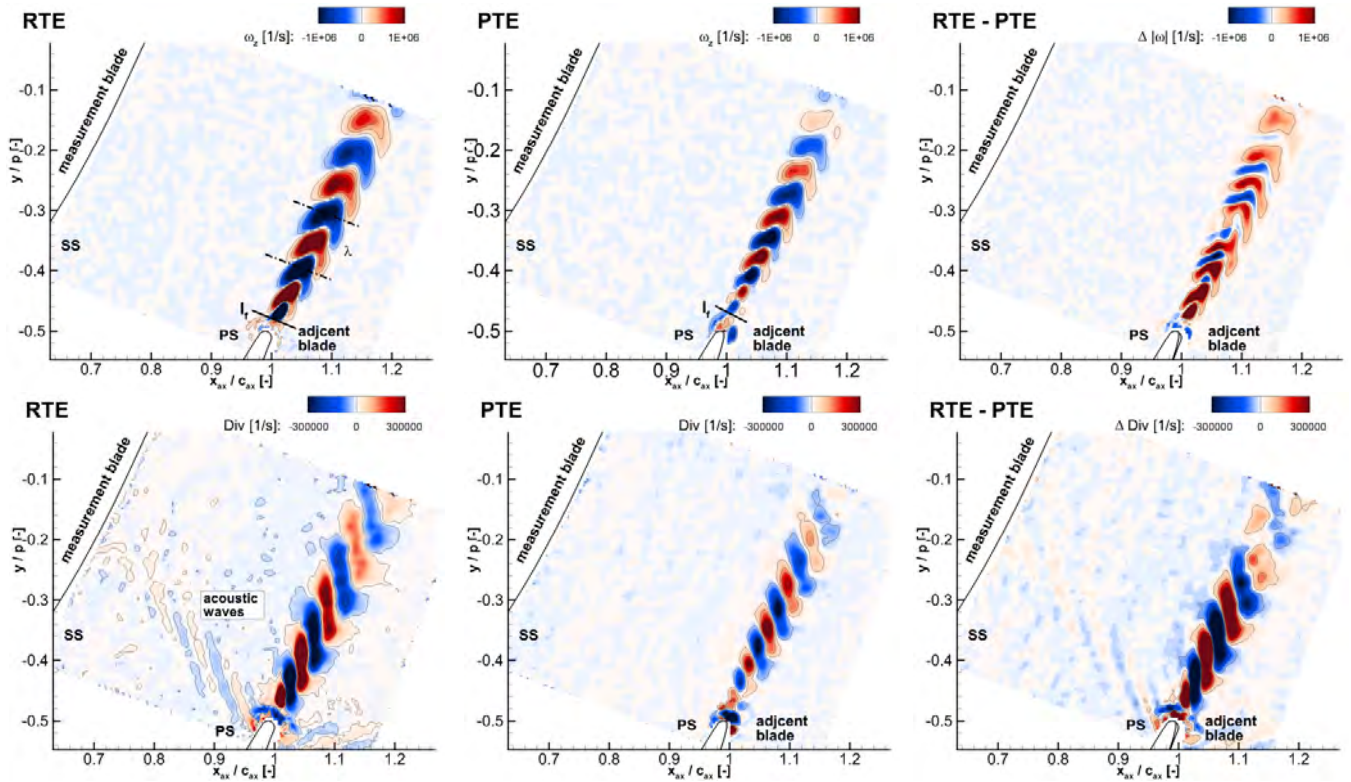
Fig.9 Spatial POD modes containing the wake for RTE, PTE and the Δ RTE - PTE (from left to right) at Ma_{2th} = 0.94 in terms of vorticity ω_z (upper row) and divergence (lower row).
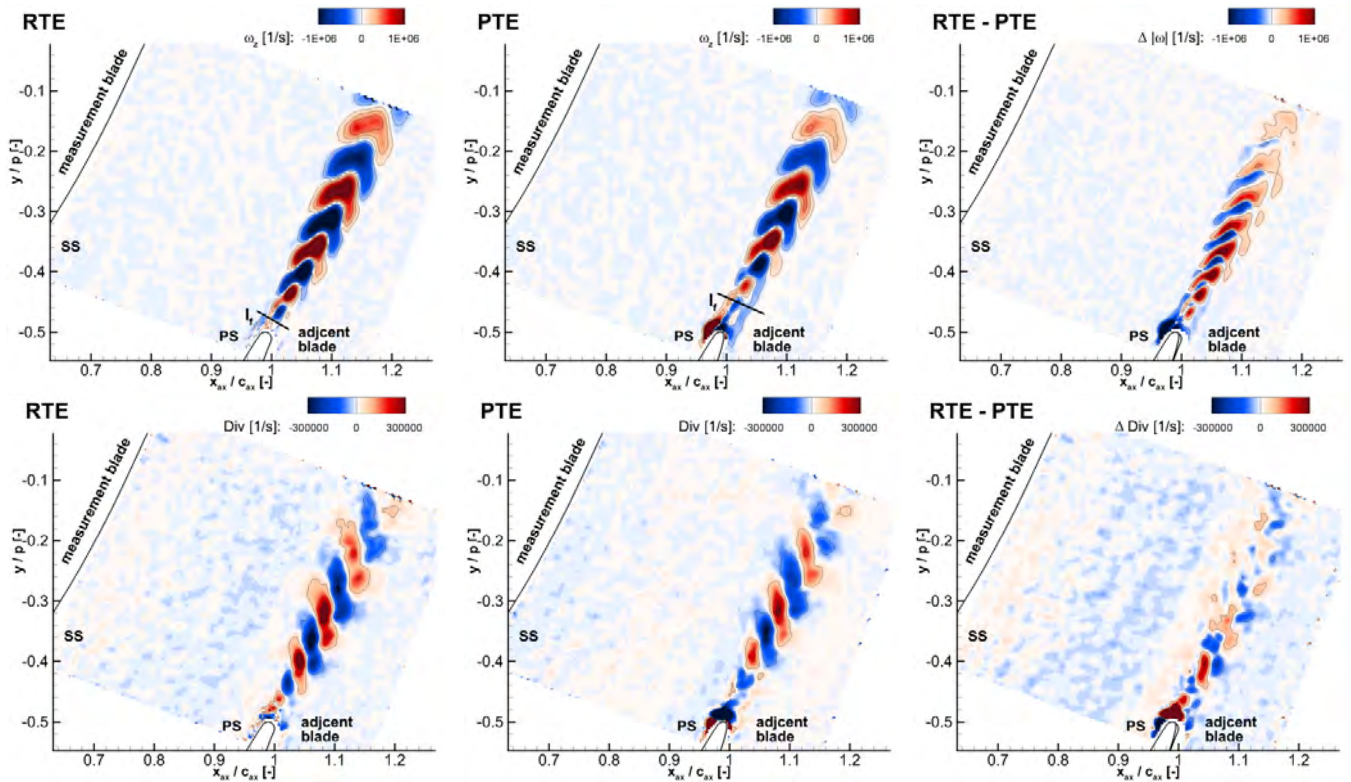

Fig.10 Spatial POD modes containing the wake for RTE, PTE and the Δ RTE - PTE (from left to right) at Ma_{2th} = 1.10 in terms of vorticity ω_z (upper row) and divergence (lower row).

PTE to approximately 37 kHz. This is in accordance with the HS-Schlieren frequency analysis where for RTE a vortex shedding frequency corresponds to a broad band peak stretching around 21 to 28 kHz. For PTE the vortex shedding frequency was higher than 31 kHz and could not be resolved with the applied sampling frequency. When looking at the divergence of the mode (lower row) for the RTE passage flow (left), the upstream propagation of acoustic wave originating at the suction and pressure side of the adjacent blade trailing edge as marked by the black ellipsis can be detected. The display of the vector field divergence is chosen because it's the quantity that depicts the propagation of the acoustic waves from both side of the adjacent trailing edge most clearly. Their periodic movement through the passage and the impingement position on the measurement blade suction side at about 74 % axial chord is visible. The upstream propagation of the acoustic waves is restricted by the local velocity reaching supersonic speed. The velocity fluctuations generated by the acoustic waves are significantly weaker and more difficult to identify than the density fluctuations visualized in the HS-Schlieren images presented in Gohl et al. [10]. No acoustic waves are visible for PTE which is in accordance with the Schlieren visualization where very weak density fluctuations in this region were discovered.

The spatial POD modes picturing the periodic vortex shedding at $Ma_{2th} = 1.10$ are depicted in Fig.10 in terms of vorticity (upper row) and divergence (lower row) for RTE, PTE and the Δ RTE-PTE (from left to right). The wake topology is similar to $Ma_{2th} = 0.94$ and resembles the alternating structure of the von Kármán vortex street for both trailing edge geometries. In comparison to $Ma_{2th} = 0.94$, the vortex formation length is extended. The vortex formation for RTE starts at a distance of 1.5 times the RTE trailing edge diameter while for PTE the starting point is delayed and located at a distance of around 4 times the PTE trailing edge diameter. The growth of the vortex formation length is expected is as the base region structure undergoes a transformation with increasing exit Mach numbers. The base region structure at $Ma_{2th} = 1.10$ will resemble more and more the triangular shape which is characterized by an isobaric base pressure and which boundaries are defined by the suction and pressure side shear layer meeting in the point of confluence. Additionally, for PTE a strong vortex pair is recognizable on the adjacent blade pressure side and on top of the base region which correlates with the vortex street. In the difference image of the vorticity magnitude Δ RTE-PTE (right)

this vortices seems to have the strongest vorticity. Apart from that, the comparison displays in general higher vorticity for RTE. The vortex shedding frequency according to Taylor's hypothesis for RTE is estimated to about 33 kHz and for PTE to approximately 35 kHz. In the modes divergence (lower row) no signs of the acoustic waves is recognizable for both trailing edge shapes. As they were visible for PTE in the Schlieren images they are probably to weak to be captured in the velocity field. The wake structure for both exit Mach number has a similar topology and the differences between the two trailing edge shapes are present at both exit Mach numbers.

Fig.11 shows the spatial modes which capture an oblique shock forming on the suction side of the measurement blade for RTE at $Ma_{2th} = 0.94$. Here the axial (upper row) and tangential velocity (lower row) are displayed. This oblique shock is visible in the normalized velocity contours depicted in Fig.5 by the abrupt termination of the suction peak triangle and its effect can also be seen in the pressure distribution in Fig.4 by the deceleration after the suction peak. The coupling between the oblique shock and the acoustic waves emerging when the main flow interacts with the formation of the vortex street at the adjacent blade trailing edge is also highlighted in this mode. About the underlying mechanism causing the oblique shock only speculations can be made. The HS-Schlieren images indicate a laminar boundary layer at the oblique shock position. The boundary layer at the impingement position of the acoustic waves is therefore objected to a periodically changing back pressure of (probably) small amplitude. The locally oscillating pressure seems to interact with the laminar boundary layer, properly increasing instabilities in the laminar layers of the boundary layer thus leading to a thickening of the boundary layer. As a consequence, the oblique shock is generated in order to redirected the flow around the thickening boundary layer. Clearly this phenomena is highly unsteady. A lot of literature was found on the impact of acoustic waves on SWBLI especially in connection with transonic buffet. But little reference was detected elucidating the effect of acoustic waves shed from the adjacent blade on boundary layer. Seguí et al. [18] reported of boundary layer instabilities induced by the acoustic waves of the adjacent blade but no oblique shock was caused by the acoustic waves. In contrast to the self-sustained shock oscillation of transonic buffet no feed-back loop between the oblique shock at the measurement blade and
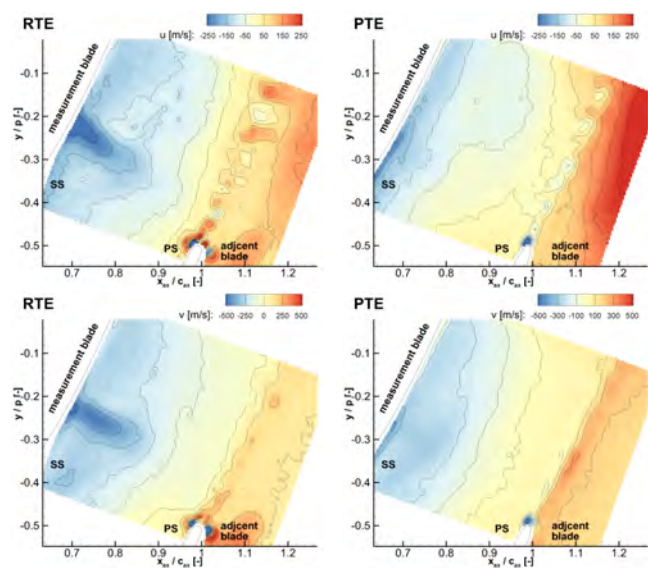

Fig.11 Spatial POD modes capturing the SWBLI and the resulting shock at the suction side of the measurement at $Ma_{2th} = 0.94$.
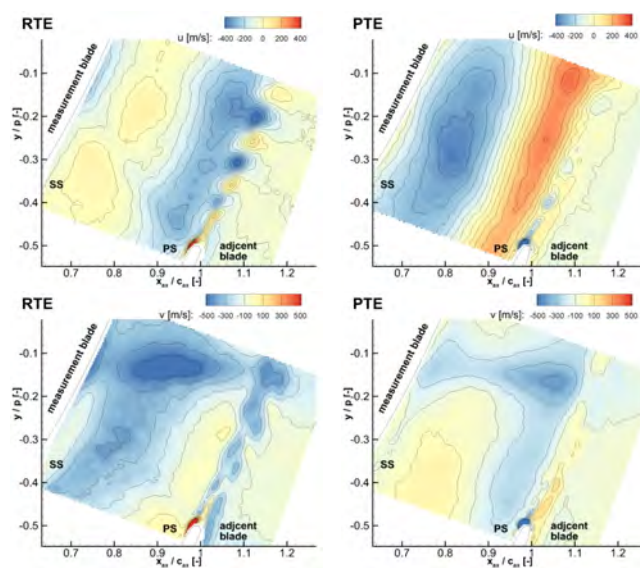

Fig.12 Spatial POD modes capturing the SWBLI and the resulting shock at the suction side of the measurement at $Ma_{2th} = 1.10$.

the acoustic waves originating at the adjacent blade is formed in this test case. Thus, a significant difference between these two phenomena exists. For Ma_{2th} = 1.10 POD modes displaying the shock system establishing in the throat region can be seen in Fig.12 for RTE and PTE (from left to right) in terms of the axial (left) and tangential velocity (right). In this mode the oblique shock formed in the throat is captured in the axial velocity. For RTE it extends over the entire passage, whereas for PTE it is limited to about half of the passage and is merely visible. The reflection of the oblique shock and the SWBLI at the measurement blade are visible in the tangential velocity field. For PTE the reflected shock seems weaker than for RTE.

CONCLUSION

An experimental investigation on a high pressure turbine cascade with cooling air ejection and two different trailing edge shapes was presented. Aerodynamic characteristics occurring in the passage of a conventional round trailing edge (RTE) and a profiled trailing edge (PTE) shape were compared for transonic exit Mach numbers ranging from Ma_{2th} = 0.80 to 1.10 while the exit Reynolds number was set constant to Re_{2th} = 1,200,000. The passage flows were investigated by the application of profile pressure tabs, wake traverse measurements using a miniaturized five-hole wedge probe as well as planar PIV. The results indicate that the PTE exhibits performance benefits from Ma_{2th} = 0.80 up to 1.00. For exit Mach numbers higher Ma_{2th} = 1.00 the loss trend is reversed and thus RTE causes less losses than PTE. Exemplary the PIV flow contours of two exit Mach numbers (Ma_{2th} = 0.94 and 1.10) were further evaluated. The TKE evolution in the wake was analyzed and it was detected that less TKE is present for PTE compared to RTE. Insight into the flow mechanisms were gained by the application of a POD analysis and the analysis of coherent structures. Two flow regions with disparate behavior were identified for RTE and PTE. The main difference of the RTE and PTE passage flows was found to occur in the wake. The second flow region that distinguishes the RTE and PTE flow is located in the throat. For RTE acoustic waves originating at the trailing edge of the neighboring blade interact with the boundary layer of the measurement blade such that an oblique shock is formed.

To conclude the results, the performance advantage of the PTE up to Ma_{2th} = 1.00 is mainly attributed to the mitigation of secondary losses arising from the shear layer oscillation at the trailing edge of the adjacent blade and the establishment of an oblique shock at the measurement blade as well as a smaller wake width. At Ma_{2th} = 1.10 the prevailing loss generating mechanism is suspected to be the trailing edge (main) shock which is stronger for PTE than for RTE thus causing higher losses.

ACKNOWLEDGEMENTS

REFERENCES

[1] Sieverding, C. H., Stanislas, M., and Snoeck, J., 1980, "The Base Pressure Problem in Transonic Turbine Cascades", *ASME J. Eng. Power,* **102**(3), pp. 711–718.

[2] Sieverding, C. H., Richard, H., and Desse, J.-M., 2003, "Turbine Blade Trailing Edge Flow Characteristics at High Subsonic Outlet Mach Number", *ASME J. Turbomach.,* **125**(2), pp. 298–309.

[3] Bölcs, A., and Sari, O., 1991, "A New Base Pressure Correlation for Transonic and Supersonic Flows", *ASME 1991 International Gas Turbine.*

[4] Prust, H. W., Jr., and Bartlett, W. M., 1974, "Cold-Air Study of the Effect on Turbine Stator Blade Aerodynamic Performance of Coolant Ejection from Various Trailing Edge Slot Geometries. 1: Experimental Results", *Nasa Technical Memoradum.*

[5] Laskowski, G. M., Kopriva, J., Michelassi, V., Shankaran, S., Paliath, U., Bhaskaran, R., Wang, Q., Talnikar, C., Wang, Z. J., and Jia, F., 2016, "Future Directions of High Fidelity CFD for Aerothermal Turbomachinery Analysis and Design", In 46th AIAA Fluid Dynamics Conference.

[6] El-Gendi, M. M., Lee, S. W., Joh, C. Y., Lee, G. S., Soon, C. H., and Chung, W. J., 2013, "Elliptic Trailing Edge for a Turbine Blade: Aerodynamic and Aerothermal Effects", *Trans. Japan Soc. Aero. S Sci.,* **56**(2), pp. 82–89.

[7] Melzer, A. P., and Pullan, G., 2019, "The Role of Vortex Shedding in the Trailing Edge Loss of Transonic Turbine Blades", *ASME J. Turbomach.,* **141**(4).

[8] Granovskiy, A., Kostege, M., and Vassiliev, V., 2014, "Effect of Unguided Turning Angle and Trailing Edge Shape on Cooled Blade Loss", In Proceedings of the ASME Turbo Expo: Turbine Technical Conference and Exposition - 2014, H. Hodson, ed., ASME.

[9] Lin, D., Su, X., and Yuan, X., 2018, "The Development and Mechanisms of the High Pressure Turbine Vane Wake Vortex", *Journal of Engineering for Gas Turbines and Power,* **140**(9).

[10] Gohl, I., Bitter, M., Kožulović, D., Sato, H., and Niehuis, R., eds., 2021, Experimental investigation on the influence of the trailing edge shape in a film cooled transonic high pressure turbine cascade, Vol. ISABE-2021-032.

[11] Niehuis, R., and Bitter, M., 2021, "The High-Speed Cascade Wind Tunnel at the Bundeswehr University Munich after a Major Revision and Upgrade", *Int. J. Turbomach. Propuls. Power,* **6**(4), p. 41.

[12] Hamabe, M., Mamada, A., Yamawaki, R., and Hamazaki, H., 2016, "Turbine Blade", IHI Corporation, Patent no.: Us9371734b2.

[13] Börner, M., and Niehuis, R., 2018, "Development of an Additive Manufactured Miniaturized Wedge Probe Optimized for 2D Transonic Wake Flow Measurements", *XXIV Biannual Symposium on Measuring Techniques in Turbomachinery.*

[14] Amecke, J., 1967, "Auswertung von Nachlaufmessungen an ebenen Schaufelgittern", *Aerodynamische Versuchsanstalt Göttingen*(67 A 49).

[15] Sirovich, L., 1987, "Turbulence and the dynamics of coherent structures, Parts I, II and III", *Quarterly of Applied Mathematics,* **45**(3), pp. 573–582.

[16] Han, L. S., and Cox, W. R., 1983, "A Visual Study of Turbine Blade Pressure-Side Boundary Layers", *Journal of Engineering for Power,* **105**(1), pp. 47–52.

[17] Lawaczeck, O., and Heinemann, H.-J., 1976, "Von Kármán Vortex Street in the Wake of Subsonic and Transonic Cascades", In *Unsteady Aerodynamics.* ARGARD CP 177, Neuilly-Sur-Seine, France.

[18] Seguí, L. M., Gicquel, L. Y. M., Duchaine, F., and de Laborderie, J., 2018, "Importance of Boundary Layer Transition in a High-Pressure Turbine Cascade Using LES", In Proceedings of the ASME Turbo Expo: Turbomachinery Technical Conference and Exposition - 2018, The American Society of Mechanical Engineers.